Regulating interfacial chemistry in lithium-ion batteries by a weakly-solvating electrolyte

Yu-Xing Yao
Tsinghua University https://orcid.org/0000-0001-6350-1206
Xiang Chen
Tsinghua University
Chong Yan
Beijing Institute of Technology https://orcid.org/0000-0001-9521-4981
Xue-Qiang Zhang
Beijing Key Laboratory of Green Chemical Reaction Engineering and Technology, Department of Chemical Engineering, Tsinghua University, Beijing 100084, P.R. China
Wen-Long Cai
Tsinghua University
Jia-Qi Huang
Beijing Institute of Technology https://orcid.org/0000-0001-7394-9186
Qiang Zhang (zhang-qiang@mails.tsinghua.edu.cn)
Tsinghua University https://orcid.org/0000-0002-3929-1541

Article

Keywords: lithium-ion battery, interfacial chemistry, weakly-solvating electrolyte, WSE, electrolyte engineering

Posted Date: July 30th, 2020

DOI: https://doi.org/10.21203/rs.3.rs-46256/v1

Version of Record: A version of this preprint was published at Angewandte Chemie on November 19th, 2020. See the published version at https://doi.org/10.1002/ange.202011482.

Regulating interfacial chemistry in lithium-ion batteries by a weakly-solvating electrolyte

Yu-Xing Yao[1], Xiang Chen[1], Chong Yan[2], Xue-Qiang Zhang[1], Wen-long Cai[1], Jia-Qi Huang[2] and Qiang Zhang*[,1]

[1]Beijing Key Laboratory of Green Chemical Reaction Engineering and Technology, Department of Chemical Engineering, Tsinghua University, Beijing 100084, China

[2]Advanced Research Institute of Multidisciplinary Science, Beijing Institute of Technology, Beijing 100081, China

Abstract: The performance of lithium-ion battery is highly dependent on its interfacial chemistry, which is regulated by electrolytes. Conventional electrolyte typically contains polar solvents to dissociate Li salts. Here, we report a novel weakly-solvating electrolyte (WSE) that consists of a pure non-polar solvent, which leads to a peculiar solvation structure where ion pairs and aggregates prevail under a low salt concentration of 1.0 M. Importantly, WSE forms unique anion-derived interphases on graphite electrodes that exhibit fast-charging and long-term cycling characteristics. First-principles calculations unravel a general principle that the competitive coordination between anions and solvents to Li ion is the origin of different interfacial chemistries. By bridging the gap between solution thermodynamics and interfacial chemistry in batteries, this work opens a brand-new way towards precise electrolyte engineering for energy storage devices with desired properties.

The Nobel Prize in Chemistry 2019 finally rewarded the development of Li-ion batteries (LIBs) as this light-weight, rechargeable, and ubiquitous energy storage device has profoundly revolutionized our modern life during the past 30 years.[1-3] The increasing demands of electric vehicles and grid energy storage is gradually pushing the performance of LIBs to their limits, including high energy density, fast charging, high safety, long life and low cost.[4-8] To meet these high bars, current LIBs must venture into more challenging territories such as Li/Si anodes,[9-11] high-voltage/capacity cathodes,[12-14] and aqueous LIBs.[15-17] Eventually, the challenges for these aggressive battery chemistries are partially or completely passed on to designing advanced electrolytes.[18] The electrolytes in LIBs not only serve as an ionic conductor, but also largely determine the electrode/electrolyte interfacial chemistry.[19] Because the performance of LIBs is strongly dependent on the electrode/electrolyte interface, developing state-of-the-art electrolytes is essential to live up to the high technological expectations.

It is well-established that the interfacial chemistry on electrodes is closely correlated to the solvation structure of electrolytes. In conventional dilute electrolytes, Li ions are usually solvated by strongly-solvating polar solvents and most anions are excluded from the solvation sheath (Fig. 1a).[19-21] Since the primary solvation sheath is the precursor of solid electrolyte interphase (SEI), such solvation structure leads to solvent-derived interfacial chemistry.[22-24] For example, the indispensable role of ethylene carbonate (EC) in modern LIBs originates from its preferential solvation and reduction which creates an exclusive EC-derived SEI to support reversible Li^+ intercalation in graphite. One major innovation of unconventional electrolytes in the past decade is the concept of superconcentrated electrolyte (SCE), with salt concentration (>3.0 M) far beyond conventional electrolytes (~1.0 M, required by the optimum conductivity).[25,26] Unlike the solvent-dominated solvation structure in dilute electrolytes, anions inevitably appear in the primary solvation sheath of Li^+ to form ion pairs or aggregates because of the scarcity of solvents and abundance of anions (Fig. 1a).[27,28] Such solvation structure leads to anion-derived SEI that enables high-rate and long-term cycling of graphite and Li metal electrodes.[29,30] Considering the high cost and viscosity

of SCE, diluting SCE with non-polar solvents emerged in recent years as an alternative to mitigate these issues.[31-33] The diluted SCE is termed localized superconcentrated electrolytes (LSCE) because the local solvation structure of LSCE is very similar to that of SCE, and therefore they belong to the same methodology.

Because solvent and anion can both serve as ligands to coordinate with Li^+ through ion–dipole or ion–ion interactions, the actual solvation structure depends on the competitive coordination between them.[34] In dilute electrolytes, solvents usually outnumber anions and hence dominate the solvation sheath of Li^+. To achieve anion-derived interfacial chemistry, the straightforward strategy is to increase the ratio of anion to solvent as in SCE or LSCE (Fig. 1a). However, is this the only way towards anion-derived interfacial chemistry?

A more essential approach towards anion-derived interfacial chemistry involves tuning the intrinsic solvating power of solvents. Because solvents and anions are competing to enter the solvation sheath of Li^+, reducing the solvating power of solvents can theoretically allow more anions to coordinate with Li^+. The ideal scenario (Fig. 1a) is a weakly-solvating electrolyte (WSE) that generates abundant ion pairs or aggregates under low salt concentrations. While SCE and LSCE are extensively studied, WSE is rarely visited because solvents with low solvating power usually can not even dissolve enough Li salts. This contradiction therefore has left this area blank, with some potentially important concepts and theories of electrolyte undiscovered.

In this work, we successfully prepared a WSE and systematically studied its solvation structure as well as interfacial chemistry on electrodes. Particularly, ultra-low solvating power and moderate Li salt solubility are simultaneously achieved in a specific solvent (1,4-dioxane) despite the apparent contradiction. Spectroscopic results confirm that WSE exhibits a peculiar solvation structure, in which ion pairs and aggregates prevail under a standard Li salt concentration of 1.0 M. Such solvation structure leads to an anion-derived, inorganic-rich SEI on graphite electrode, which allows for fast Li^+ transport. First-principles calculations unravel a fundamental rationale that the relative binding energy between anions/solvents and Li^+ dictates the electrode/electrolyte

interfacial chemistry, which blazes a new trail in precise electrolyte design for future batteries.

Results and discussion

Model System: Fig. 1b lists the dielectric constant (ε, also known as permittivity) of various solvents used in this study, which is a key indicator of the solvating power of solvents. In the carbonate family, EC possesses an extremely high ε of 89.8 as a strongly solvating solvent and dominates the primary solvation sheath of Li^+. The Li^+–coordinated EC is then reduced on graphite electrode to form a desirable SEI, which is contributed by the typical solvent-derived interfacial chemistry. In this study, commercial electrolyte consisting of EC/methyl ethyl carbonate (EMC) (1:2, v/v) mixed solvents and 1.0 M LiFSI serves as the control sample and is denoted as EC/EMC. Three ethers, dimethoxyethane (DME), 1,3-dioxane (1,3-DX), and 1,4-dioxane (1,4-DX) with ε of 7.0, 13.0, and 2.2, respectively, are chosen as the model system to induce a transition from solvent-derived interfacial chemistry to anion-derived interfacial chemistry based on solvating power regulation (Fig. 1c). DME has the largest solvating power among the three solvents despite the moderate ε, because it has a chelating effect on Li^+.[35,36] 1,3-DX exhibits lower solvating power due to the steric effect caused by its cyclic structure. The most extreme case and the protagonist in this study, 1,4-DX, possesses an ultra-low ε even lower than that of benzene (ε=2.3), which are both typical non-polar solvents. Theoretically, 1,4-DX should have an extremely weak solvating power. Actually, lithium hexafluorophosphate ($LiPF_6$) is almost insoluble in 1,4-DX， and lithium bis(trifluoromethylsulphonyl)imide (LiTFSI) also exhibits a very limited solubility (<0.3 M) although these two salts possess a high solubility and are commonly adopted in battery research or industrial applications (Fig. S1a and b). Interestingly, lithium bis(fluorosulfonyl)imide (LiFSI) is found to be the only soluble Li salt in 1,4-DX, exhibiting a maximum solubility up to 2.0 M (Fig. S1c) and conceivably forming a unique solvation structure. To ensure that solvating power is the only controlled variable in this study, all electrolytes were formulated with 1.0 M LiFSI as Li salt and

denoted as the name of their solvents. The elaborately designed electrolyte series, namely DME, 1,3-DX, and 1,4-DX, should represent a decreasing trend of solvating power and increasing trend of ion pair formation.

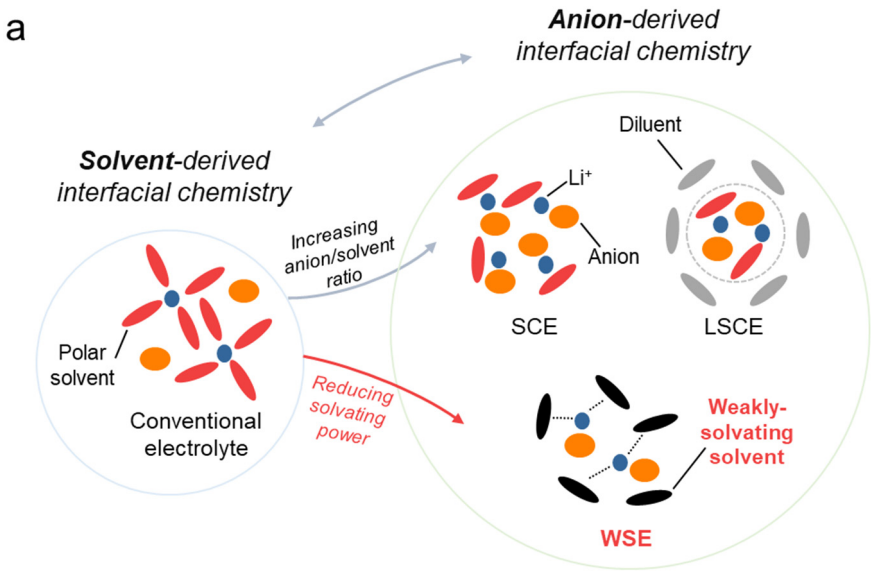

b

Solvent	Dielectric constant
EC	89.8
EMC	2.9
DME	7.2
1,3-DX	13.0
1,4-DX	2.2
benzene	2.3

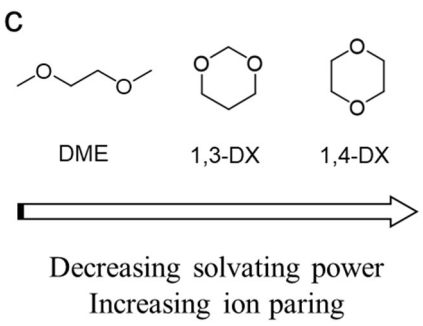

Fig. 1. a) Schematics of the solvation structures in conventional electrolyte, superconcentrated electrolyte (SCE), localized superconcentrated electrolyte (LSCE) and weakly-solvating electrolyte (WSE). b) Dielectric constant of various solvents. c) The ranking of solvating power of solvents from high to low.

Solvation Structure: The solvation structures of the above-mentioned electrolytes were investigated by spectroscopic characterizations combined with first-principles calculations. Raman spectra were first obtained for three ether-based electrolytes (Fig. 2a and S2). As shown in Fig. 2a, The S–N–S bending signal in FSI^- anion can be classified into three distinctive bands: free anion (FA, 719.0 cm^{-1}, non-coordinated

FSI^-), contact ion pair (CIP, 730.6 cm^{-1}, one FSI^- binding with one Li^+), and ion aggregate (AGG, 742.3 cm^{-1}, one FSI^- binding with two or more Li^+).[37] The specific portion of these three species were calculated from the peak area and listed in Fig. 2b.[28] DME electrolyte contains 71.3% of FA, 28.7% CIP, and no AGG, indicating that most anions are expelled from the primary solvation sheath due to the strong solvating power of DME. Accordingly, a new vibration band of DME solvent at 800–900 cm^{-1} arises (Fig. S2a), which signifies the abundant Li^+–DME complexes. In 1,3-DX with less solvating power, the ratio of FA significantly reduces as the ratio of CIP and AGG increases. The additional band of 1,3-DX vibration in Fig. S2b indicates that considerable Li^+–1,3-DX complexes are still present. Surprisingly, the weakly-solvating 1,4-DX electrolyte contains merely 15.6% of FA, and the solvation structure is dominated by CIP (49.0%) and AGG (35.4%). Raman vibration bands of pure 1,4-DX and 1.4-DX electrolyte are almost identical (Fig. S2b), indicating that the interaction between 1,4-DX and Li^+ is extremely weak. Nevertheless, the solubility of LiFSI in 1,4-DX is still sufficiently high. This counterintuitive result suggests that LiFSI becomes a weak electrolyte and largely undissociated in sparingly-solvating 1,4-DX solvent, although it is regarded as a strong electrolyte in conventional solvents due to the very weak interaction between Li^+ and charge-delocalized FSI^-.

The ^{17}O nuclear magnetic spectroscopy (^{17}O-NMR) analysis confirms the same trend of transition of the solvation structure (Fig. 2c and S3). When the long pair electrons in anions or solvents coordinate with Li^+, it results in a shielding effect on the electronic environment of ^{17}O nuclei which is subsequently expressed by the upfield displacement of chemical shifts in NMR spectra.[38] The chemical shift of ^{17}O nuclei in LiFSI molecules decreases in the order of DME > EC/EMC > 1,3-DX > 1,4-DX, indicating that the coordination between Li^+ and FSI^- should follow the reverse trend. The above preliminary results show that a WSE is indeed constructed exactly as designed when LiFSI is dissolved in 1,4-DX. As a direct correlation, when the solvating power of solvent reduces, solvents in the primary solvation sheath are gradually replaced by anions.

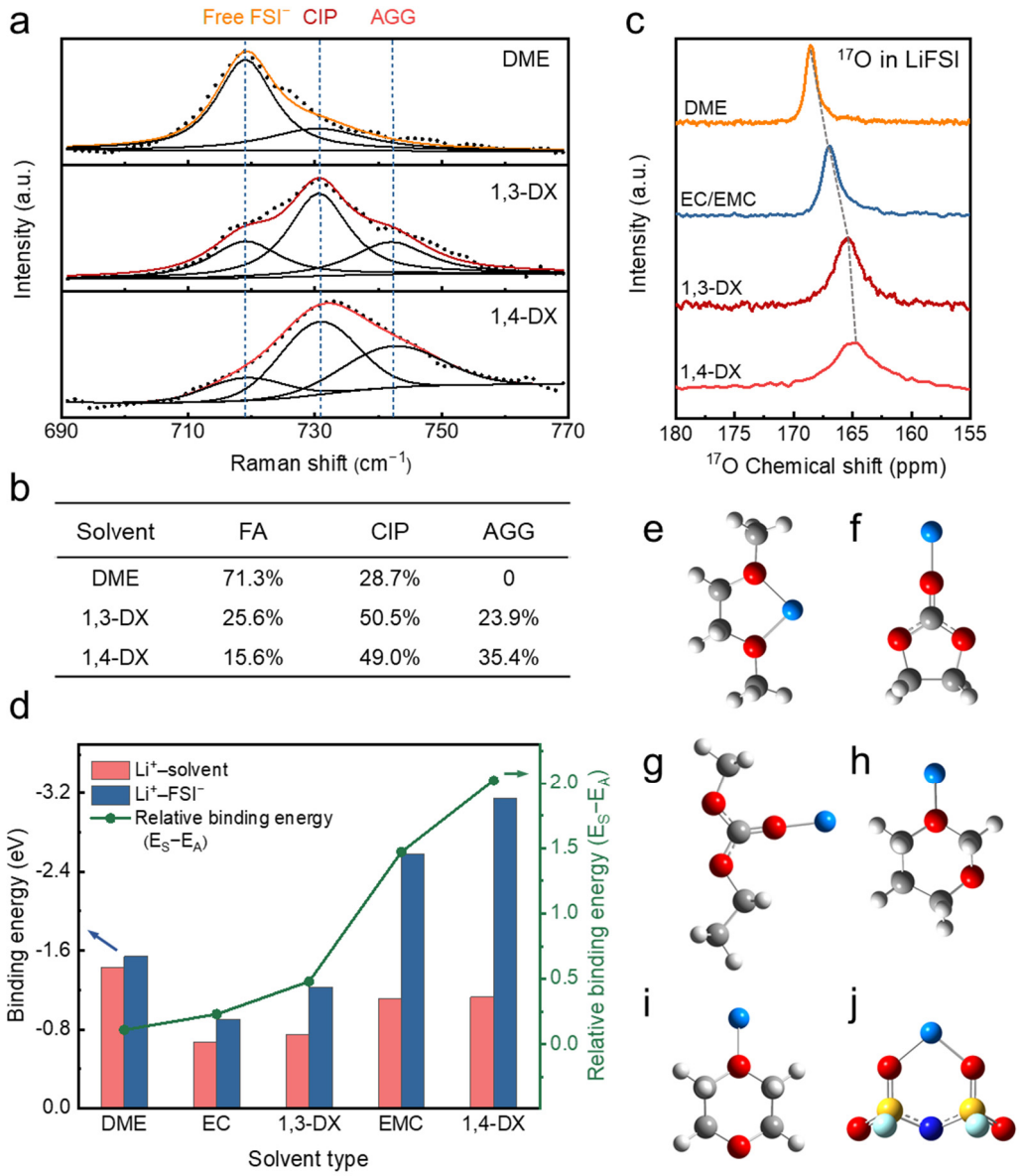

Solvent	FA	CIP	AGG
DME	71.3%	28.7%	0
1,3-DX	25.6%	50.5%	23.9%
1,4-DX	15.6%	49.0%	35.4%

Fig. 2. The evolution of solvation structure by regulating the solvating power of solvents. a) Raman spectra of 1.0 M LiFSI dissolved in various solvents. b) The ratio of different solution structures in various solvents calculated from a). c) Natural abundance ^{17}O NMR spectra of 1.0 M LiFSI dissolved in various solvents. Signals were collected at 60℃. d) The binding energies between Li+ and solvents/anions obtained by first-principles calculations. The corresponding optimized geometrical structures of e) Li^+–DME, f) Li^+–EC, g) Li^+–EMC, h) Li^+–1,3-DX, i) Li^+–1,4-DX, j) Li^+–FSI^-. H white, Li blue, C grey, O red, S yellow, N dark blue, F light blue.

To elucidate the origin of different solvation structures, first-principles calculations were further conducted to probe the molecular interactions between anions/solvents and

Li^+ (Fig. 2d–2j and Table S1), which are expressed in terms of binding energy. The binding energy of Li^+–solvent (E_S) and Li^+–anion (E_A) complexes is primarily determined by two major factors: *1) The chemical structure of the ligands.* Typically, carbonyl O exhibits higher nucleophilicity than ethereal O, therefore carbonates usually have higher solvating power than ethers. Moreover, ligands with multiple coordination sites (also known as the chelating effect) exhibit stronger interaction with Li^+ than monodentate ligands. For example, DME and FSI^- both have two O atoms coordinated with Li^+ (Fig. 2e and 2j), therefore exhibit larger binding energies (e.g., E_S = −1.43 eV for DME). The coulombic attraction between Li^+ and FSI^- contributes to an even stronger interaction and thus larger E_A compared to E_S. *2) The dielectric constant of the solution.* Large dielectric constant of solvents weakens the Li^+–anion and Li^+–solvent interactions, which can be approximately described by classical physical models:[34]

$$U_{ion-ion} = \frac{-1}{4\pi\varepsilon} \times \frac{q_1 q_2}{r} \quad (1)$$

$$U_{ion-dipole} = \frac{-1}{4\pi\varepsilon} \times \frac{q\mu cos\theta}{r^2} \quad (2)$$

where ε is the dielectric constant, q the charge of ion, μ the dipole moment of dipole, r the distance between ion and ion or ion and the center of dipole, and θ the dipole angle relative to the line r joining the ion and the center of the dipole. For instance, the relatively low E_S of EC (−0.67 eV, which seems contradictory to its high solvating power) is due to its large ε (89.8), and the extremely high E_A (−3.15 eV) in 1,4-DX is due to its small ε (2.2) that inhibits salt dissociation. Interestingly, if the binding energy of Li^+–EC is calculated in 1,4-DX environment (which practically means to add a small amount of EC in 1,4-DX that does not change the solvent environment), the E_S of Li^+–EC (−1.38 eV) is significantly larger than the E_S of Li^+–1,4-DX (−1.13 eV). According to the above analyses, it is unreasonable to directly compare E_S or E_A in different electrolytes because it does not reveal direct information on the solvation structure of a particular electrolyte. On the other hand, analyzing the value of E_S and E_A in the same electrolyte environment affords fresh insights on the competitive coordination between anions and solvents with Li^+.

The descriptor of E_S-E_A is further proposed to predict the actual solvation structure in different electrolytes. By definition, a larger E_S-E_A indicates that the ion pair and aggregate are preferentially formed over Li^+–solvent complexes, namely that anions win the coordination competition over solvents. Fig. 2d illustrates that the trend of E_S-E_A (DME < EC < 1,3-DX < 1,4-DX) is in perfect accordance with spectroscopic results, which strongly affirms the applicability of the descriptor of E_S-E_A. As a rule of thumb, large numbers of Li^+–solvent complexes and free anions are anticipated for E_S-E_A close to 0 (such as in DME); ion pairs and aggregates prevail for extremely large E_S-E_A (>2.0 eV, such as in 1,4-DX); Li^+–solvent complex and ion pair jointly constitute the solvation structure for intermediate E_S-E_A (0.5–1.5 eV, such as in 1,3-DX). The most striking significance to emerge from E_S-E_A is that it serves as a quantitative indicator to predict to what extent do anions intrude the primary solvation sheath of Li^+. Our theory reveals the underlying mechanism that different solvation structures originate from the competitive coordination between solvents and anions towards a thermodynamically stable Li^+ solvation sheath.

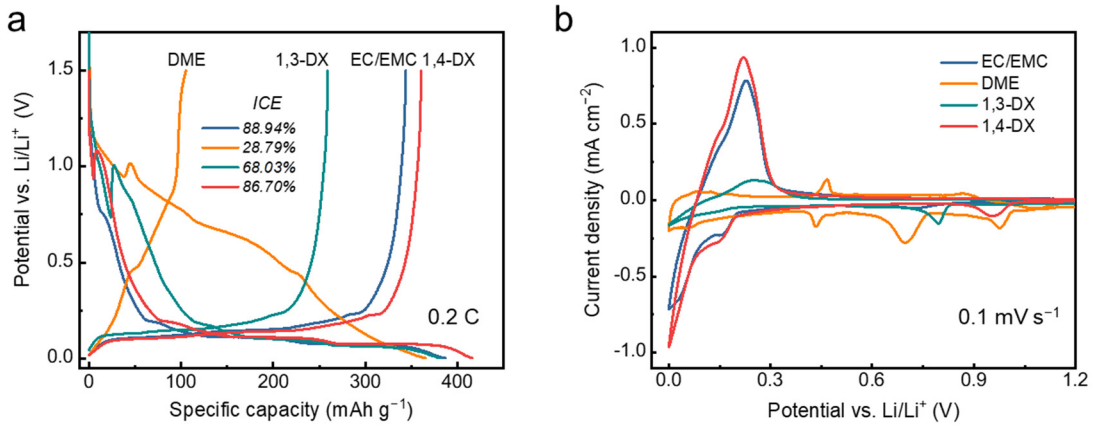

Fig. 3. Electrochemical behavior of graphite electrodes in various neat solvents containing 1.0 M LiFSI. a) First cycle charge–discharge curves and b) first-cycle CV curves of graphite electrodes in various electrolytes.

Li^+ Intercalation Behavior in Graphite: To explore the effect of different solvation structures on the interfacial chemistry of electrodes, graphite electrode is chosen as a

touchstone because the reversible Li^+ intercalation in graphite is highly sensitive to the solvation structure of Li^+ in bulk electrolyte.[39,40] Fig. 3a and 3b exhibits the charge/discharge curves and cyclic voltammetry (CV) curves of graphite during the first cycle in different electrolytes. EC is strongly coordinated with Li^+ and reduced at ~0.8 V *vs.* Li/Li^+ to form a stable SEI in the EC/EMC electrolyte (Fig. S4), which is a typical case of solvent-derived interfacial chemistry. Graphite lithiation/delithiation in EC/EMC is highly reversible, with three voltage plateaus between 0.05–0.25 V representing the different stages of Li–graphite intercalation compounds. Unlike carbonates, ethers have long been regarded as unstable against graphite electrode.[19] DME electrolyte causes severe co-intercalation at 0.4–1.0 V that undermines the structure of layered graphite (Fig. S5) so that reversible lithiation can not be achieved. This is because DME are also strongly coordinated with Li^+, but is unable to form stable SEI that prevents co-intercalation. This phenomenon is common for ether-based electrolytes, as 1,3-DX also exhibits slight co-intercalation, sluggish lithiation kinetics, and an initial coulombic efficiency (ICE) of merely 68.03%. Although the co-intercalation of 1,3-DX is milder than that of DME because of the weaker solvating power and higher degree of ion pair formation (Fig. S5), the reversibility of graphite lithiation is still unsatisfactory. Surprisingly, 1,4-DX electrolyte exhibits a high reversible capacity of 360.5 mAh g^{-1} and faster lithiation/delithiation kinetics even exceeding the commercial EC/EMC electrolyte. The ICE of 1,4-DX (86.7%) is close to that of EC/EMC (88.94%), implying that 1,4-DX electrolyte leads to a stable SEI formation. To the best of our knowledge, this is the first report of highly reversible lithiation of graphite in neat ether electrolytes without applying superconcentration or any additives. This unexpected phenomenon is attributed to the unique solvation structure of the 1,4-DX electrolyte, where the prevailing ion pairs and aggregates leads to preferential reduction of anions (at ~1.0 V, Fig. 3b and S4) to form an anion-derived SEI. In order to verify this postulation, a detailed investigation on the SEI of graphite is prerequisite.

Interfacial Chemistry and Kinetics: The surface passivation film on graphite (SEI) is the key to reversible Li^+ intercalation.[41] The Li^+ intercalation behavior of graphite indicates that only two electrolytes can form stable SEI and enable reversible lithiation: the commercial EC/EMC electrolyte and the 1,4-DX electrolyte (also denoted as WSE). XPS is conducted to characterize the composition and structure of SEI on graphite in these two electrolytes and study the SEI formation mechanisms. The deconvolution of C 1s spectra reveals four peaks (Fig. 4a), representing C–C (284.8 eV, from graphite), C–O (286.6 eV), C=O (288.8 eV), and C–F (290.1 eV, from PVDF binder). The peak intensities of C–O and C=O in WSE are significantly lower than that of EC/EMC, indicating a suppressed solvent decomposition in WSE compared to the EC decomposition in EC/EMC that generates abundant organic species in SEI.

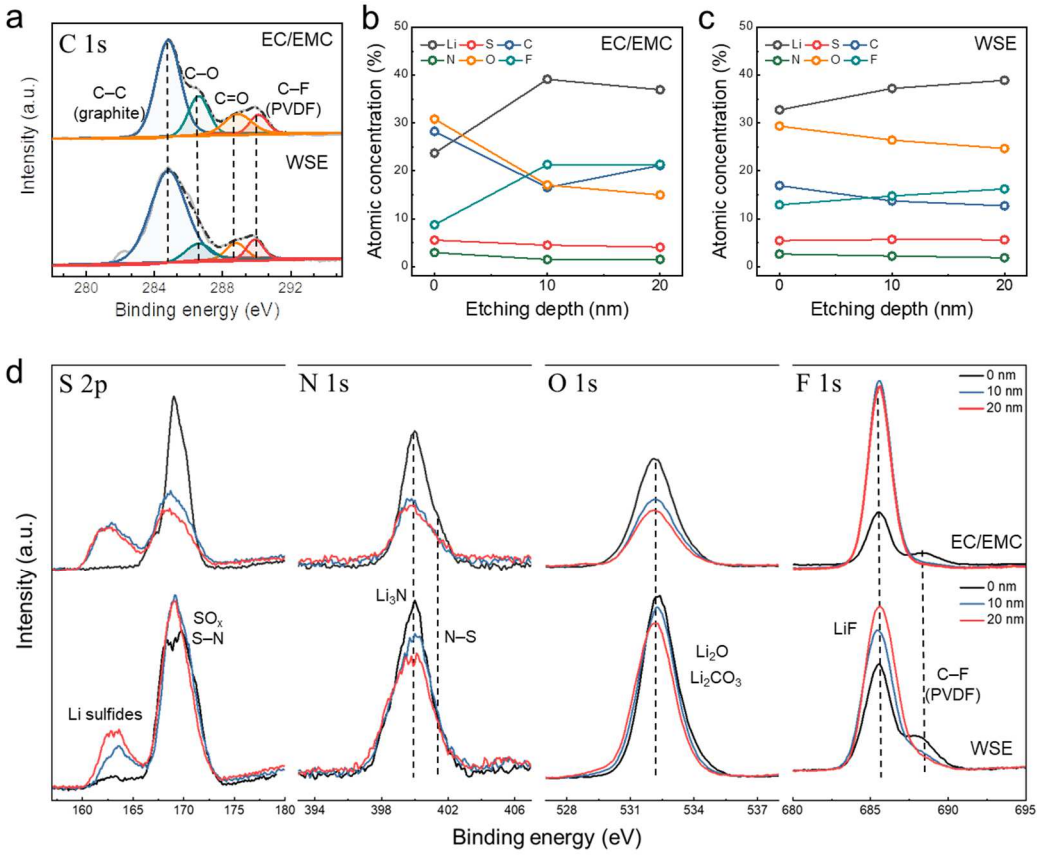

Fig. 4. Interfacial chemistry of graphite electrodes in EC/EMC and WSE electrolyte revealed by XPS depth profiling after 5 formation cycles. a) C 1s spectra of SEI on graphite electrodes. Atomic concentration at different depths of SEI in b) EC/EMC electrolyte and c) WSE electrolyte. d) S 2p, N 1s, O 1s, F 1s spectra of SEI on graphite electrodes at different depths.

The atomic concentration at different etching depths reveals the structure of SEI (Fig. 4b and 4c). The etching depth corresponds to the standard thermal oxidation of SiO_2 samples. For EC/EMC, the C and O concentrations sharply decrease from 0 to 10 nm as the F content increases, then stabilize from 10 to 20 nm. This result is in accordance with the classic two-layer SEI model, in which the outer layer mainly consists of organic species at higher oxidation state (mainly Li alkyl carbonates) and the inner layer consists of various inorganic compounds (LiF, Li_2CO_3, and N, S-containing species as shown in Fig. 4d) that are more stable against reduction.[42] Therefore, SEI is mainly solvent-derived in EC/EMC electrolytes, accompanied by partial anion reduction. In contrast, the atomic contents in WSE-derived SEI are almost constant from 0 to 20 nm with lower C content and more inorganic ingredients, indicating that the SEI is highly homogeneous along its depth and inorganic in nature. A closer examination reveals that the O content in WSE-derived SEI is roughly twice of the F content, which is exactly the stoichiometric ratio in FSI^-. Therefore, in WSE the SEI is generated mainly through anion reduction that generates abundant inorganic species such as LiF, Li_2O, Li_3N, Li sulfide, and Li oxysulfide (Fig. 4d), etc. The XPS results confirm that EC/EMC features solvent-derived interfacial chemistry and WSE features anion-derived interfacial chemistry.

Temperature-dependent electrochemical impedance spectroscopy (EIS) were employed to determine the kinetics of different interfacial processes. Three-electrode setup using a Li@Cu reference electrode was implemented to accurately measure the impedance signal of graphite electrode without the complication of the Li counter electrode (Fig. 5a, S6a, and S6b). Based on a well-established theory, the semicircle at mid-frequency region in the Nyquist plot represents the desolvation step of Li^+ (known as the charge transfer impedance) and the semicircle at high-frequency region represents Li^+ transport through SEI (Fig. 5b).[43,44] The EIS spectra were fitted according to the classic Arrhenius law and activation energies of each interfacial process are obtained (Fig. 5b and 5c). WSE shows a slightly reduced Li^+ desolvation energy barrier ($E_{a,\,ct}$ = 48.2 kJ mol^{-1}) compared to EC/EMC ($E_{a,\,ct}$ = 54.7 kJ mol^{-1}). Since the Li^+–

solvent interaction is much weaker in WSE than in EC/EMC as previously demonstrated, such reduction of Li^+ desolvation energy barrier may seem insignificant. However, since the Li^+–FSI^- interaction in WSE is much stronger than in EC/EMC, desolvation is mainly contributed by the dissociation of ion pairs and aggregates which is also energy-consuming.[45] Most importantly, the activation energy for Li^+ transport through SEI in WSE ($E_{a,\,SEI}$ = 26.6 kJ mol^{-1}) is significantly lower than in EC/EMC ($E_{a,\,SEI}$ = 44.7 kJ mol^{-1}). This is because the inorganic species dispersed in anion-derived SEI creates abundant phase boundaries and vacancies for rapid Li^+ diffusion, which prominently reduce the energy barrier. In the solvent-derived SEI, Li^+ undergoes pore diffusion in the outer layer, which requires a higher activation energy and renders limited kinetics. The kinetics analysis implies that the unique anion-derived interphase may potentially enable fast-charging characteristic.

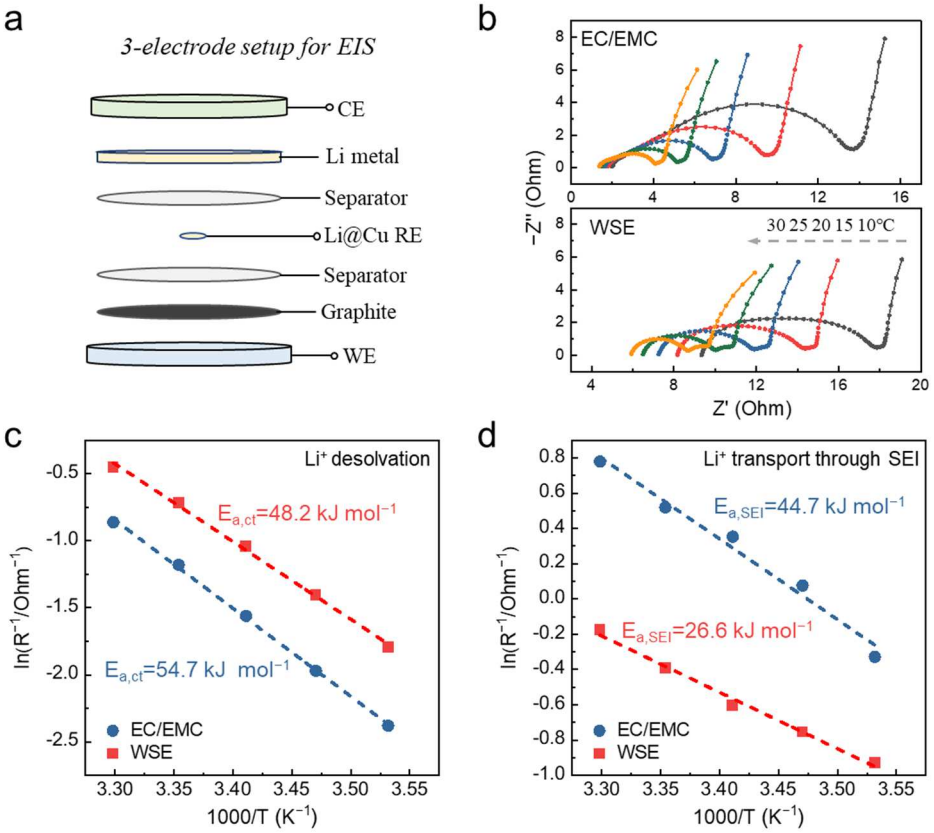

Fig. 5. Kinetics of interfacial processes at the graphite/electrolyte interface measured by EIS using a 3-electrode setup. a) Cell configuration of 3-electrode setup for EIS measurements. b) Temperature-dependent EIS curves of cells containing EC/EMC and WSE. c) Arrhenius

behavior of the resistance corresponding to Li^+ desolvation. d) Arrhenius behavior of the resistance corresponding to Li^+ transport through SEI.

Electrochemical Performance: To understand the role of different interfacial chemistries in the electrochemical performance of electrodes, both rate and cycling tests were conducted for graphite electrodes in EC/EMC and WSE electrolytes. The WSE exhibits a remarkable fast-charging performance even far exceeding the commercial EC/EMC electrolyte (Fig. 6a and b), retaining 54% of its capacity even at a demanding rate of 4 C. The charging process can be divided into 4 steps: 1) Li^+ diffusion through pores in the graphite electrode, 2) Li^+ desolvation at the electrolyte/electrode interfaces, 3) Li^+ transport through SEI, and 4) Li diffusion within graphite galleries. It is obvious that process 4 is identical in EC/EMC and WSE. Because the ionic conductivity of WSE is nearly one-magnitude lower than that of EC/EMC (Fig. S7) due to the lack of Li salt dissociation, step 1 can not be the reason for its outstanding rate performance. Consequently, the exceptional rate performance of WSE is attributed to the accelerated Li^+ desolvation step induced by its unique solvation structure, and rapid Li^+ diffusion through the anion-derived SEI. This conclusion is supported by the interfacial kinetics analysis. In other words, even the conductivity of WSE is substantially smaller, its anion-derived interfacial chemistry induces rapid kinetics of Li^+ migration across interfaces and the impressive fast-charging capability.

Long term cycling of graphite electrodes at 1 C rate were carried out straight after the rate tests to examine the SEI stability (Fig. 6c, S8a and S8b). EC/EMC exhibits a 78% capacity retention after 300 cycles, which is acceptable for routine EC-based electrolytes without any additive. However, WSE renders a rapid capacity decay during long term cycling and only retains 34% of its initial capacity after 300 cycles. This phenomenon is attributed to the fragile nature of inorganic-rich SEI derived from anion decomposition. The anion-derived SEI is broken under high stress due to the volume fluctuation of graphite during cycling. This leads to the repeated cracking and repair of SEI that gradually increase its thickness overtime, which finally result in a growing resistance and capacity fade. On the contrary, the organic SEI layer in EC/EMC

possesses higher elasticity and is more resilient to mechanical deformations, therefore offers a better protection of the graphite electrode.

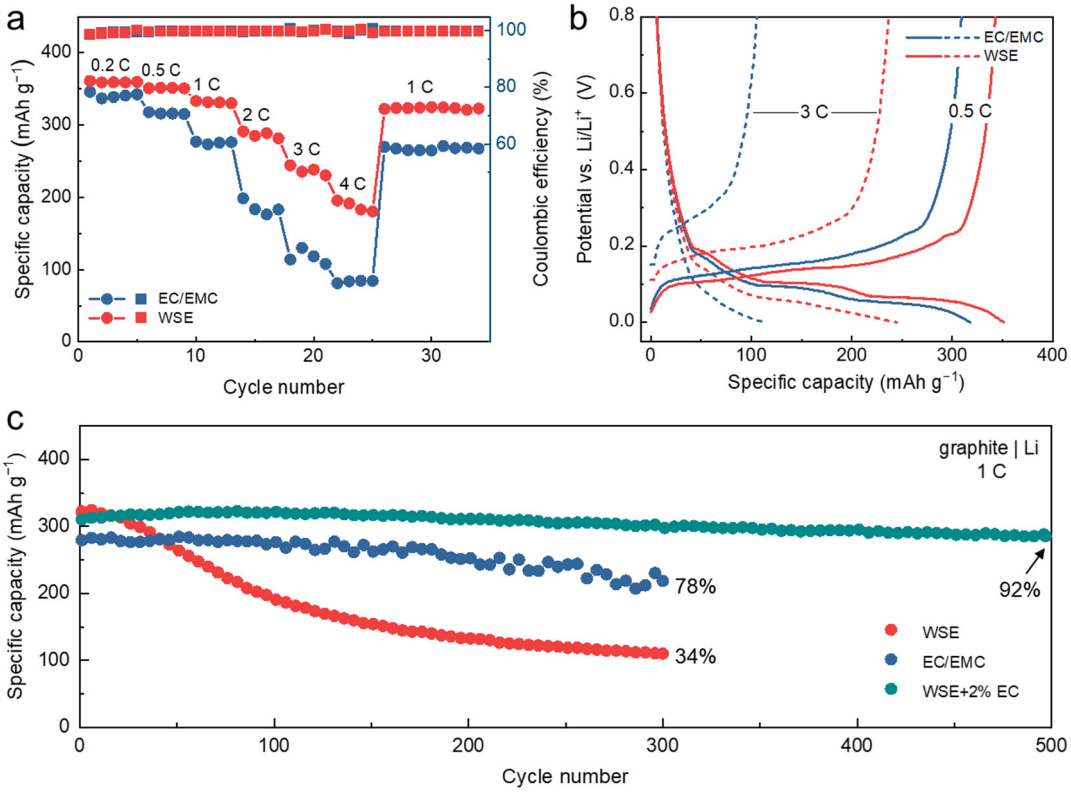

Fig. 6. Electrochemical performance of graphite electrode in different electrolytes. a) Specific capacity of graphite electrodes in EC/EMC and WSE under various charge and discharge rates. b) The corresponding charge and discharge curves at selected rates. c) Long term cycling performance of graphite electrode in EC/EMC, WSE and WSE+2% EC electrolyte at 1 C charge and discharge rate. Long term cycling tests were conducted after the rate tests without interval.

Interestingly, the fragility of anion-derived SEI and the poor cycling performance of WSE can be overcome by exploiting the competitive coordination between solvents and anions. As previously shown, the binding energy between Li^+ and EC is large in 1,4-DX environment (−1.38 eV, Fig. S4). Simply by adding 2.0 wt% EC into WSE (denoted as WSE + 2% EC), some EC molecules will coordinate with Li^+ and replace a small part of ion pairs and aggregates. Consequently, these EC molecules are reduced

on graphite electrodes to produce a small number of organic compounds that infiltrate into the inorganic compounds, which serves as the glue to enhance the stability of SEI. As a result, WSE+2% EC enables ultra-stable cycling of graphite electrode with 92% capacity retention after 500 cycles (Fig. 6c and S8c), and retains a satisfactory rate performance (Fig. S9). If the cell was directly cycled at 1 C without the rate test, a longer life exceeding 840 cycles can be obtained with 80% capacity retention (Fig. S10). Such superior cycling performance is very rare for graphite electrodes in ether-based electrolytes, further demonstrating the huge potential of anion-derived interfacial chemistry achieved by solvating power regulation.

Conclusions

In summary, a completely new route towards anion-derived interfacial chemistry in LIBs is developed. Unlike superconcentrated electrolytes, the essence of this methodology is constructing a weakly-solvating electrolyte by using a non-polar but salt-dissolving solvent. WSE exhibits a peculiar solvation structure where ion pairs and aggregates prevail under a low salt concentration of 1.0 M. As a result, the anion-derived SEI exhibits superior interfacial charge transport kinetics and high stability, enabling fast-charging and long-term cycling of graphite electrodes. First-principles calculations unravel the fundamental rationale that the competitive coordination between solvents and anions controls the transition from solvent-derived interfacial chemistry to anion-derived interfacial chemistry. Furthermore, a semi-empirical descriptor was put forward to predict the actual solvation structure in electrolytes. This work constitutes the first step of an undiscovered way towards anion-derived interfacial chemistry, in which the methodology serves as an emerging principle for coming studies on precise electrolyte engineering towards next-generation energy storage devices.

Methods

Materials: Lithium metal foil was purchased from China Energy Lithium Co., Ltd. Mesocarbon microbeads (MCMB) powder was purchased from Hefei Kejing Materials Technology Co., Ltd. Dimethoxyethane (DME), 1,3-dioxane (1,3-DX) and 1,4-dioxane (1,4-DX) were all purchased from Tokyo Chemical Industry Co., Ltd. Ethylene carbonate (EC), methyl ethyl carbonate (EMC), lithium bis(fluorosulfonyl)imide (LiFSI), lithium hexafluorophosphate ($LiPF_6$), and lithium bis(trifluoromethylsulphonyl)imide (LiTFSI) were all purchased from Duoduo Chem Co., Ltd. The solvents and Li salts were all battery-grade. Electrolytes were formulated by adding 1.0 M LiFSI into various pure solvents or mixed-solvents before vigorously stirring to ensure complete dissolution. Graphite electrodes were prepared by blade-coating method using N-methyl-2-pyrrolidone as solvent and contains 80 wt.% MCMB powder, 10 wt.% carbon black, and 10 wt.% polyvinylidene fluoride (PVDF) binder. The areal loading of graphite electrodes was about 1.4 mg cm^{-2}. Graphite electrodes were dried at 70℃ overnight and punched into disks with diameter of 13 mm before use.

Structural Characterizations: The morphology of graphite electrodes was characterized by scanning electron microscopy (SEM, JSM 7401F, JEOL Ltd., Japan) operated at 10.0 kV. X-ray photoelectron spectroscopy (XPS) results of the graphite surface film were obtained using PHI Quantera SXM (ULVAC-PHI, Inc., Kanagawa, Japan) with an Al K_α radiation (pass energy 55.0 eV) at a pressure lower than 10^{-7} torr. All graphite electrode samples were washed three times using pure DME to clean the surface residual Li salts and organic solvents before characterization. Electrolyte solution structures were characterized using Raman spectroscopy and ^{17}O nuclear magnetic spectroscopy (^{17}O-NMR). The Raman spectrometer was LabRAM HR800 (HORIBA Jobin Yvon Ltd.) with an exciting laser of 633 nm. The ^{17}O-NMR spectra were acquired on a JNM-ECA600 spectrometer with H_2O used as an external reference set to 0 ppm. NMR results were obtained at 50℃. During sample transfer process before

any characterization, all samples were sealed in Ar-filled containers to avoid direct contact with air and moisture.

Electrochemical Measurements: The graphite/Li cells were assembled in standard 2032 coin-type cells with 40 μL electrolyte in an Ar-filled glove box with both oxygen and water contents below 1.0 ppm. Electrochemical impedance spectroscopy (EIS) and cyclic voltammetry (CV) measurements were performed on Solartron 1470E electrochemical workstation (Solartron Analytical, UK). EIS measurements were performed in the frequency range from 10^5 to 10^{-1} Hz with a voltage amplitude of 10 mV. CV tests were conducted in the voltage range of 0–1.2 V at a scan rate of 0.1 mV s^{-1}. Battery charge/discharge tests were all conducted using LAND multichannel battery cycler (Wuhan LAND Electronics Co., Ltd.). The graphite/Li cells were all cycled between 0–1.5 V in the galvanostatic mode. During the rate test, cells were cycled at 0.2 C, 0.5 C, 1.0 C, 2.0 C, 3.0 C, 4.0 C and back to 1.0 C for long-term cycling.

Computational Details: First-principles calculations based on density functional theory were performed in Gaussian (G09) suite of program with Becke's three parameter hybrid method using the Lee–Yang–Parr correlation functional (B3LYP). The geometrical structures and the vibrational modes were calculated at 6-311++G(d, p) level. Meanwhile, the solvation effect was considered with integral equation formalism variant of the Polarizable Continuum (IEFPCM) model. The binding energy (E_b) between two components was defined as following:

$$E_b = E_{total} - E_A - E_B$$

where E_{total}, E_A, and E_B are the total energy of the A–B complexes, A component, and B component, respectively. A and B can be Li ion, anions, and solvents.

References

1 Yan, C. *et al.* Toward Critical Electrode/Electrolyte Interfaces in Rechargeable Batteries. *Adv. Funct. Mater.* **30**, 1909887 (2020).

2 Li, M., Lu, J., Chen, Z. & Amine, K. 30 Years of Lithium-Ion Batteries. *Adv. Mater.* **30**, 1800561 (2018).

3 Winter, M., Barnett, B. & Xu, K. Before Li Ion Batteries. *Chem. Rev.* **118**, 11433−11456 (2018).

4 Deng, J., Bae, C., Denlinger, A. & Miller, T. Electric Vehicles Batteries: Requirements and Challenges. *Joule* **4**, 511−515 (2020).

5 Zeng, X. Q. *et al.* Commercialization of Lithium Battery Technologies for Electric Vehicles. *Adv. Energy Mater.* **9**, 1900161 (2019).

6 Schmuch, R., Wagner, R., Horpel, G., Placke, T. & Winter, M. Performance and cost of materials for lithium-based rechargeable automotive batteries. *Nat. Energy* **3**, 267−278 (2018).

7 Zhu, G. L. *et al.* Fast Charging Lithium Batteries: Recent Progress and Future Prospects. *Small* **15**, 1805389 (2019).

8 Zhao, Q., Stalin, S., Zhao, C.-Z. & Archer, L. A. Designing solid-state electrolytes for safe, energy-dense batteries. *Nat. Rev. Mater.* **5**, 229−252 (2020).

9 Liu, J. *et al.* Pathways for practical high-energy long-cycling lithium metal batteries. *Nat. Energy* **4**, 180−186 (2019).

10 Cheng, X. B., Zhang, R., Zhao, C. Z. & Zhang, Q. Toward Safe Lithium Metal Anode in Rechargeable Batteries: A Review. *Chem. Rev.* **117**, 10403−10473 (2017).

11 Feng, K. *et al.* Silicon-Based Anodes for Lithium-Ion Batteries: From Fundamentals to Practical Applications. *Small* **14**, 1702737 (2018).

12 Li, W., Song, B. & Manthiram, A. High-voltage positive electrode materials for lithium-ion batteries. *Chem. Soc. Rev.* **46**, 3006−3059 (2017).

13 Liu, Q. *et al.* Approaching the capacity limit of lithium cobalt oxide in lithium ion batteries via lanthanum and aluminium doping. *Nat. Energy* **3**, 936−943 (2018).

14 Lee, J. *et al.* Reversible Mn^{2+}/Mn^{4+} double redox in lithium-excess cathode materials. *Nature* **556**, 185−190 (2018).

15 Lu, Y. & Chen, J. Prospects of organic electrode materials for practical lithium batteries. *Nat. Rev. Chem.* **4**, 127−142 (2020).

16 Yang, C. *et al.* Aqueous Li-ion battery enabled by halogen conversion–intercalation chemistry in graphite. *Nature* **569**, 245−250 (2019).

17 Suo, L. *et al.* "Water-in-salt" electrolyte enables high-voltage aqueous lithium-ion chemistries. *Science* **350**, 938−943 (2015).

18 Li, M., Wang, C., Chen, Z., Xu, K. & Lu, J. New Concepts in Electrolytes. *Chem. Rev.* (2020). DOI: 10.1021/acs.chemrev.9b00531.

19 Xu, K. Electrolytes and interphases in Li-ion batteries and beyond. *Chem. Rev.* **114**, 11503−11618 (2014).

20 Xu, K., Lam, Y. F., Zhang, S. S., Jow, T. R. & Curtis, T. B. Solvation sheath of Li+ in nonaqueous electrolytes and its implication of graphite/electrolyte interface chemistry. *J. Phys. Chem. C* **111**, 7411−7421 (2007).

21 Zhang, X. Q. *et al.* Highly Stable Lithium Metal Batteries Enabled by Regulating the Solvation of Lithium Ions in Nonaqueous Electrolytes. *Angew. Chem. Int. Ed.* **57**, 5301−5305 (2018).

22 von Cresce, A. & Xu, K. Preferential Solvation of Li^+ Directs Formation of Interphase on Graphitic Anode. *Electrochem. Solid-State Lett.* **14**, A154−A156 (2011).

23 von Wald Cresce, A., Borodin, O. & Xu, K. Correlating Li^+ Solvation Sheath Structure with Interphasial Chemistry on Graphite. *J. Phys. Chem. C* **116**, 26111−26117 (2012).

24 Xu, K. Manipulating interphases in batteries. *Natl. Sci. Rev.* **4**, 19−20 (2017).

25 Zheng, J., Lochala, J. A., Kwok, A., Deng, Z. D. & Xiao, J. Research Progress towards Understanding the Unique Interfaces between Concentrated

Electrolytes and Electrodes for Energy Storage Applications. *Adv. Sci.* **4**, 1700032 (2017).

26 Yamada, Y., Wang, J. H., Ko, S., Watanabe, E. & Yamada, A. Advances and issues in developing salt-concentrated battery electrolytes. *Nat. Energy* **4**, 269−280 (2019).

27 Sodeyama, K., Yamada, Y., Aikawa, K., Yamada, A. & Tateyama, Y. Sacrificial Anion Reduction Mechanism for Electrochemical Stability Improvement in Highly Concentrated Li-Salt Electrolyte. *J. Phys. Chem. C* **118**, 14091−14097 (2014).

28 Suo, L. *et al.* How Solid-Electrolyte Interphase Forms in Aqueous Electrolytes. *J. Am. Chem. Soc.* **139**, 18670−18680 (2017).

29 Yamada, Y. *et al.* Unusual stability of acetonitrile-based superconcentrated electrolytes for fast-charging lithium-ion batteries. *J. Am. Chem. Soc.* **136**, 5039−5046 (2014).

30 Qian, J. *et al.* High rate and stable cycling of lithium metal anode. *Nat. Commun.* **6**, 6362 (2015).

31 Chen, S. *et al.* High-Voltage Lithium-Metal Batteries Enabled by Localized High-Concentration Electrolytes. *Adv. Mater.* **30**, 1706102 (2018).

32 Ren, X. D. *et al.* Localized High-Concentration Sulfone Electrolytes for High-Efficiency Lithium-Metal Batteries. *Chem* **4**, 1877−1892 (2018).

33 Zhang, X. H. *et al.* Advanced Electrolytes for Fast-Charging High-Voltage Lithium-Ion Batteries in Wide-Temperature Range. *Adv. Energy Mater.* **10**, 2000368 (2020).

34 Chen, X., Zhang, X.-Q., Li, H.-R. & Zhang, Q. Cation−Solvent, Cation−Anion, and Solvent−Solvent Interactions with Electrolyte Solvation in Lithium Batteries. *Batteries & Supercaps* **2**, 128−131 (2019).

35 Zhang, C. *et al.* Chelate effects in glyme/lithium bis(trifluoromethanesulfonyl)amide solvate ionic liquids. I. Stability of solvate cations and correlation with electrolyte properties. *J. Phys. Chem. B* **118**, 5144−5153 (2014).

36 Ueno, K. *et al.* Li^+ solvation in glyme–Li salt solvate ionic liquids. *Phys. Chem. Chem. Phys.* **17**, 8248−8257 (2015).

37 Yamada, Y., Yaegashi, M., Abe, T. & Yamada, A. A superconcentrated ether electrolyte for fast-charging Li-ion batteries. *Chem. Commun.* **49**, 11194-11196 (2013).

38 Bogle, X., Vazquez, R., Greenbaum, S., Cresce, A. & Xu, K. Understanding Li^+−Solvent Interaction in Nonaqueous Carbonate Electrolytes with ^{17}O NMR. *J. Phys. Chem. Lett.* **4**, 1664−1668 (2013).

39 Yamada, Y., Koyama, Y., Abe, T. & Ogumi, Z. Correlation between Charge−Discharge Behavior of Graphite and Solvation Structure of the Lithium Ion in Propylene Carbonate-Containing Electrolytes. *J. Phys. Chem. C* **113**, 8948−8953 (2009).

40 Jeong, S.-K., Inaba, M., Iriyama, Y., Abe, T. & Ogumi, Z. Interfacial reactions between graphite electrodes and propylene carbonate-based solutions: Electrolyte-concentration dependence of electrochemical lithium intercalation reaction. *J. Power Sources* **175**, 540−546 (2008).

41 Peled, E. & Menkin, S. Review—SEI: Past, Present and Future. *J. Electrochem. Soc.* **164**, A1703−A1719 (2017).

42 Heiskanen, S. K., Kim, J. & Lucht, B. L. Generation and Evolution of the Solid Electrolyte Interphase of Lithium-Ion Batteries. *Joule* **3**, 2322−2333 (2019).

43 Xu, K., von Cresce, A. & Lee, U. Differentiating Contributions to "Ion Transfer" Barrier from Interphasial Resistance and Li^+ Desolvation at Electrolyte/Graphite Interface. *Langmuir* **26**, 11538−11543 (2010).

44 Xu, K. "Charge-transfer" process at graphite/electrolyte interface and the solvation sheath structure of Li^+ in nonaqueous electrolytes. *J. Electrochem. Soc.* **154**, A162−A167 (2007).

45 Sagane, F., Abe, T. & Ogumi, Z. Li^+-Ion Transfer through the Interface between Li^+-Ion Conductive Ceramic Electrolyte and Li^+-Ion-Concentrated Propylene Carbonate Solution. *J. Phys. Chem. C* **113**, 20135−20138 (2009).

Acknowledgements

This work was supported by National Natural Science Foundation of China (21825501, 21805161, and U1801257), National Key Research and Development Program (2016YFA0202500), and the Tsinghua University Initiative Scientific Research Program. The authors thank Rui Xu and Lei Xu for useful discussions.

Author contributions

Y.-X.Y. and Q.Z. conceived the idea. Q.Z. supervised the work. Y.-X.Y. designed and conducted the electrochemical measurements and materials characterizations. W.-L.C. provided experimental assistance. X.C. conducted the first-principles calculation results. C.Y. and J.-Q.H. contributed to the interpretation of data. Y.-X.Y., X.C., C.Y., X.-Q.Z. and Q.Z. co-wrote the manuscript with input from all the authors.

Competing interests

The authors declare no competing interests.

Figures

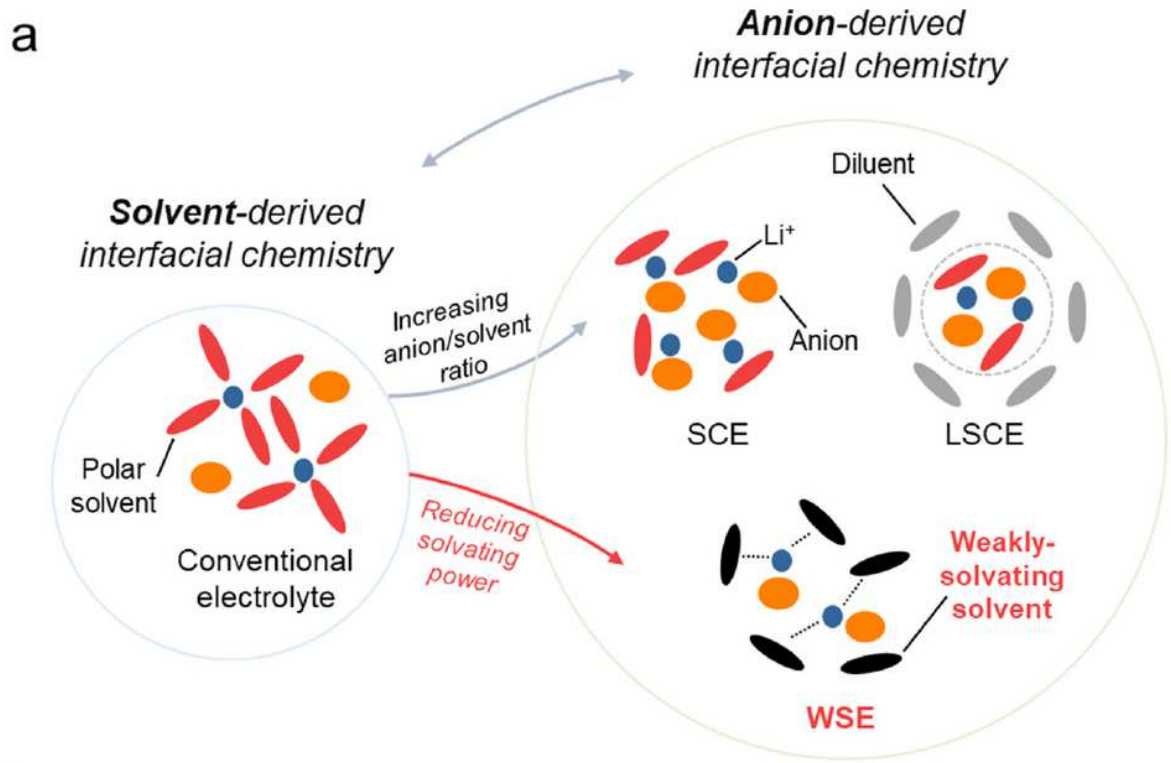

b

Solvent	Dielectric constant
EC	89.8
EMC	2.9
DME	7.2
1,3-DX	13.0
1,4-DX	2.2
benzene	2.3

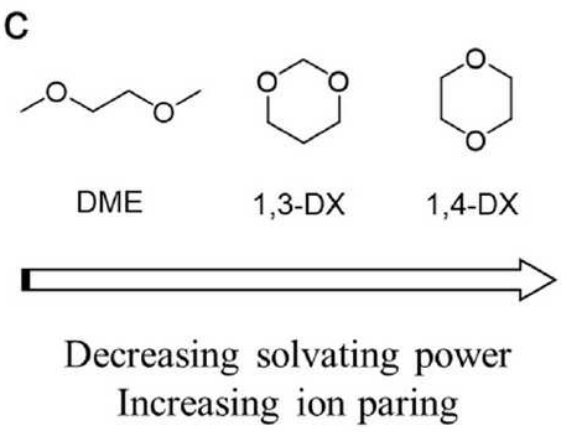

Figure 1

a) Schematics of the solvation structures in conventional electrolyte, superconcentrated electrolyte (SCE), localized superconcentrated electrolyte (LSCE) and weakly-solvating electrolyte (WSE). b) Dielectric constant of various solvents. c) The ranking of solvating power of solvents from high to low.

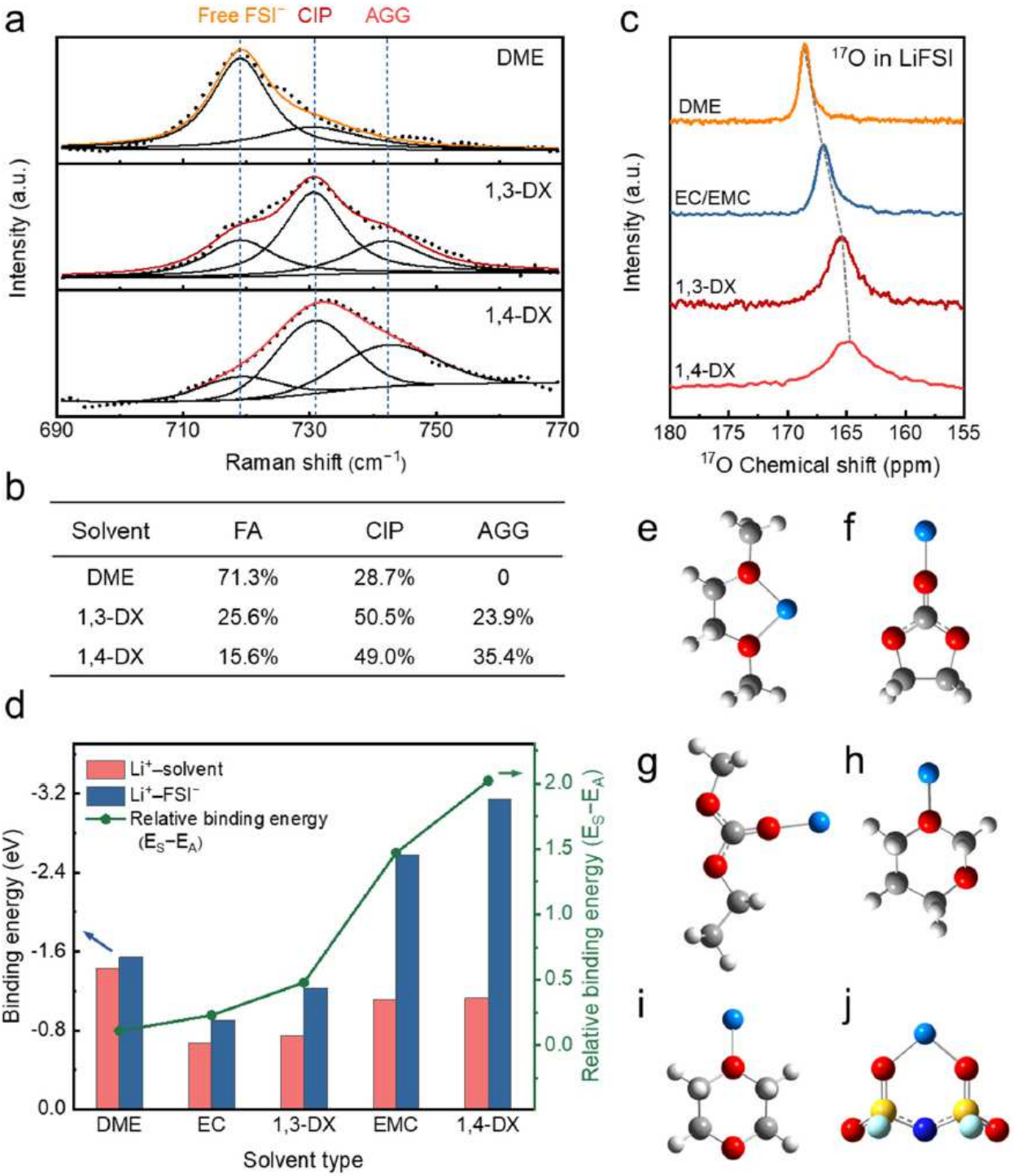

Solvent	FA	CIP	AGG
DME	71.3%	28.7%	0
1,3-DX	25.6%	50.5%	23.9%
1,4-DX	15.6%	49.0%	35.4%

Figure 2

The evolution of solvation structure by regulating the solvating power of solvents. a) Raman spectra of 1.0 M LiFSI dissolved in various solvents. b) The ratio of different solution structures in various solvents calculated from a). c) Natural abundance 17O NMR spectra of 1.0 M LiFSI dissolved in various solvents. Signals were collected at 60□. d) The binding energies between Li+ and solvents/anions obtained by first-principles calculations. The corresponding optimized geometrical structures of e) Li+–DME, f) Li+–EC, g)

Li+–EMC, h) Li+–1,3-DX, i) Li+–1,4-DX, j) Li+–FSI–. H white, Li blue, C grey, O red, S yellow, N dark blue, F light blue.

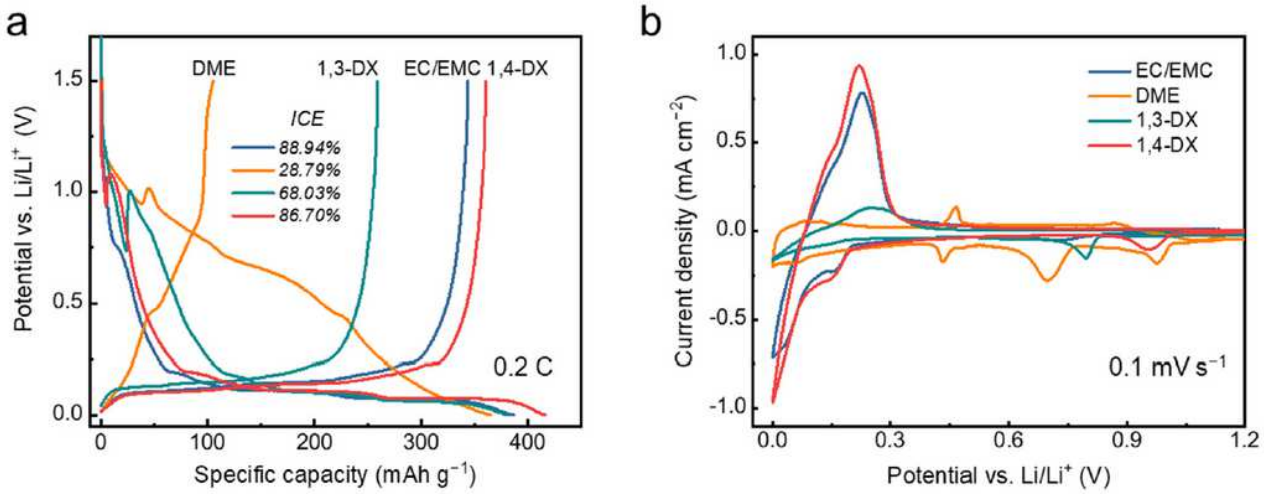

Figure 3

Electrochemical behavior of graphite electrodes in various neat solvents containing 1.0 M LiFSI. a) First cycle charge–discharge curves and b) first-cycle CV curves of graphite electrodes in various electrolytes.

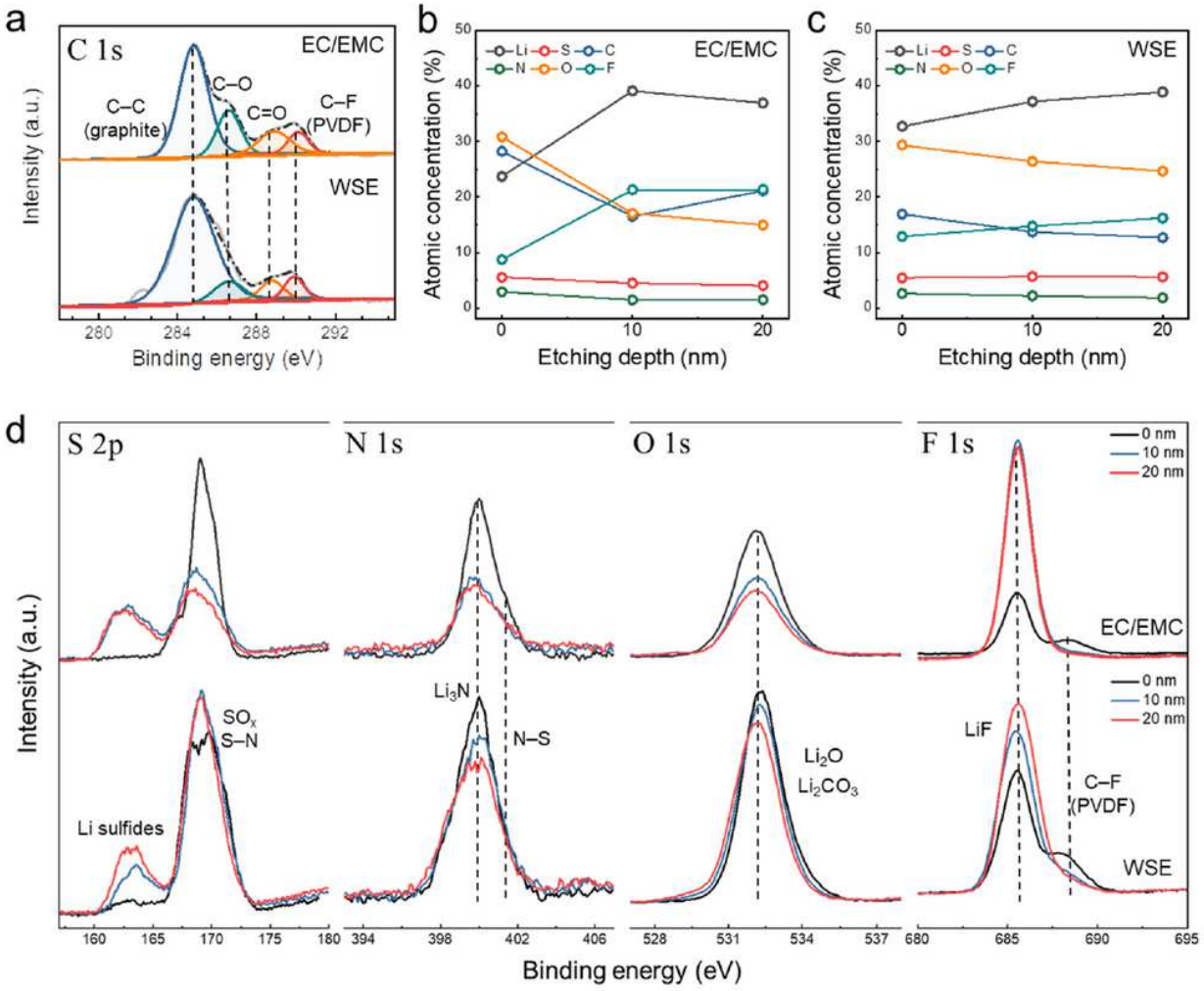

Figure 4

Interfacial chemistry of graphite electrodes in EC/EMC and WSE electrolyte revealed by XPS depth profiling after 5 formation cycles. a) C 1s spectra of SEI on graphite electrodes. Atomic concentration at different depths of SEI in b) EC/EMC electrolyte and c) WSE electrolyte. d) S 2p, N 1s, O 1s, F 1s spectra of SEI on graphite electrodes at different depths.

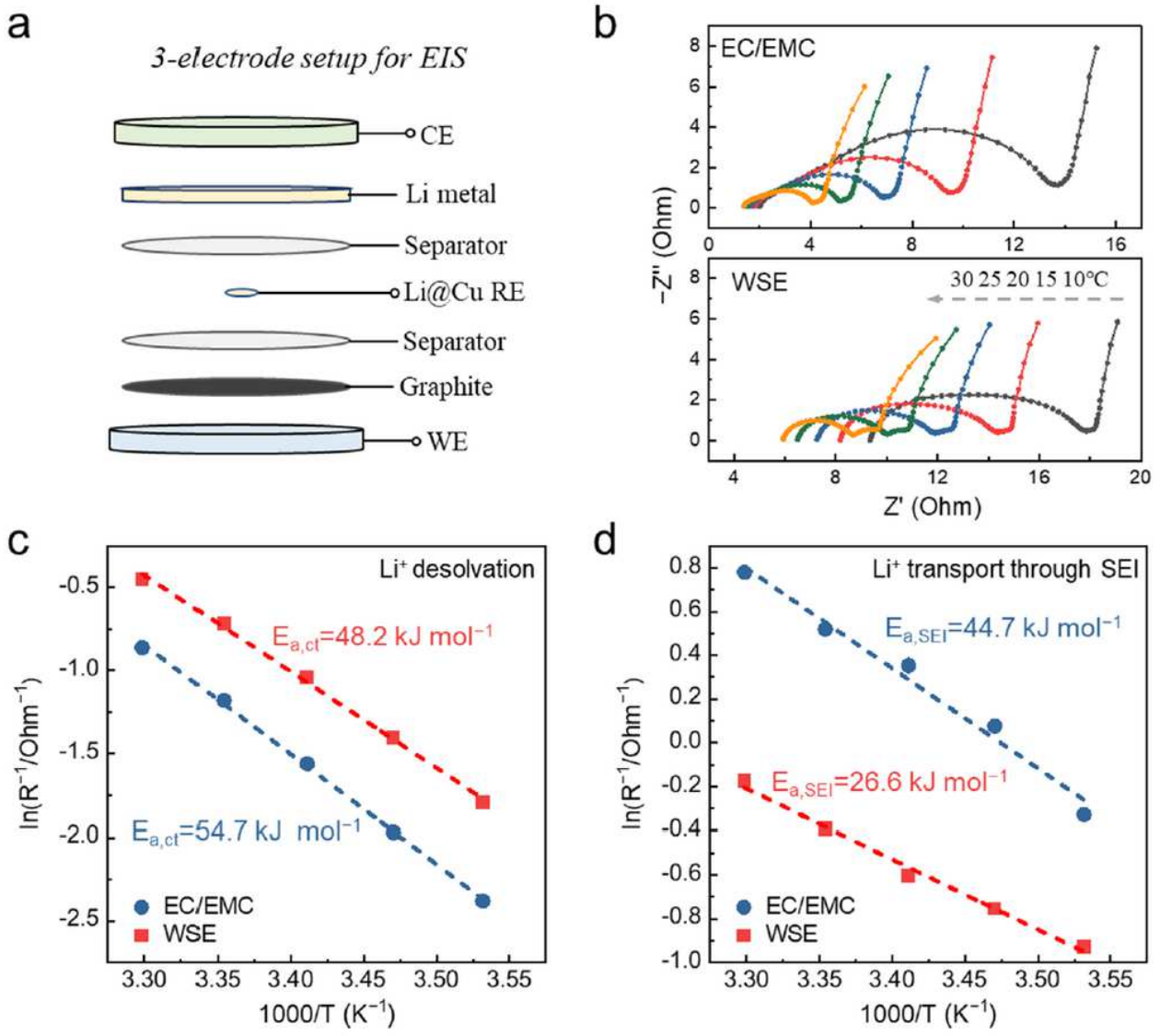

Figure 5

Kinetics of interfacial processes at the graphite/electrolyte interface measured by EIS using a 3-electrode setup. a) Cell configuration of 3-electrode setup for EIS measurements. b) Temperature-dependent EIS curves of cells containing EC/EMC and WSE. c) Arrhenius behavior of the resistance corresponding to Li+ desolvation. d) Arrhenius behavior of the resistance corresponding to Li+ transport through SEI.

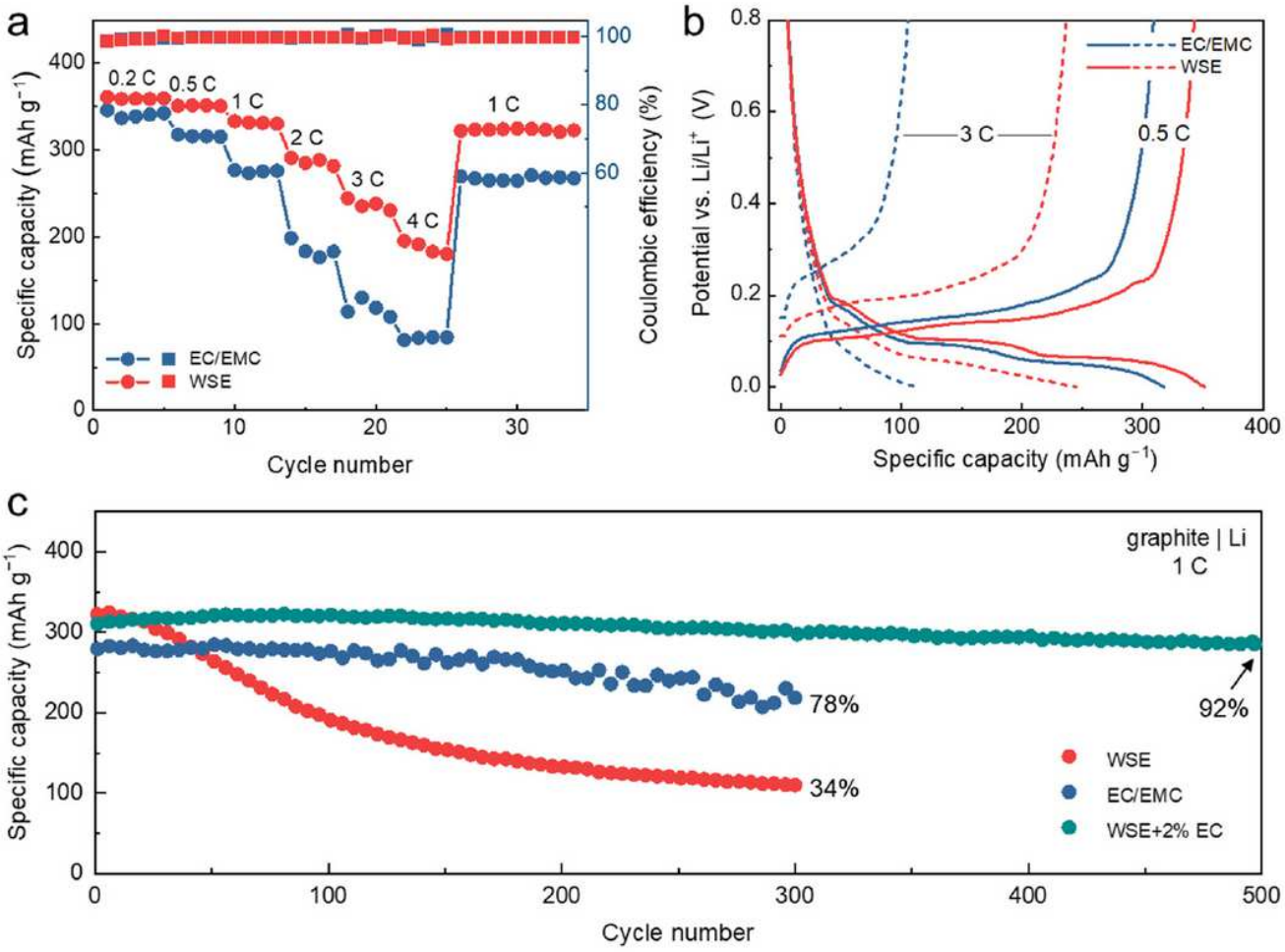

Figure 6

Electrochemical performance of graphite electrode in different electrolytes. a) Specific capacity of graphite electrodes in EC/EMC and WSE under various charge and discharge rates. b) The corresponding charge and discharge curves at selected rates. c) Long term cycling performance of graphite electrode in EC/EMC, WSE and WSE+2% EC electrolyte at 1 C charge and discharge rate. Long term cycling tests were conducted after the rate tests without interval.

Supplementary Files

This is a list of supplementary files associated with this preprint. Click to download.

- ncommsSI.pdf